Research paper

Magnetospheric Venus Space Explorers (MVSE) mission: A proposal for understanding the dynamics of induced magnetospheres

Roland Albers [1], Henrik Andrews [2], Gabriele Boccacci [3], Vasco D.C. Pires [4,5], Sunny Laddha [6], Ville Lundén [7], Nadim Maraqten [8], João Matias [9], Eva Krämer [10,*], Leonard Schulz [11], Ines Terraza Palanca [12], Daniel Teubenbacher [6,13], Claire Baskevitch [14,15], Francesca Covella [16], Luca Cressa [17], Juan Garrido Moreno [18], Jana Gillmayr [19], Joshua Hollowood [20], Kilian Huber [21,17], Viktoria Kutnohorsky [22], Sofia Lennerstrand [23], Adel Malatinszky [24], Davide Manzini [25,26], Manuel Maurer [27], Daiana Maria Alessandra Nidelea [28], Luca Rigon [29], Jonas Sinjan [30], Crisel Suarez [31,32], Mirko Viviano [7], Elise Wright Knutsen [33]

[1] Institute of Applied Physics, University of Bern, Bern, Switzerland
[2] Norwegian University of Science and Technology, Høgskoleringen 1, Trondheim, 7034, Norway
[3] Sapienza University of Rome, Rome, Italy
[4] DEMec, Faculty of Engineering, University of Porto, R. Dr. Roberto Frias, Porto, 4200-465, Portugal
[5] Chair of Designing Plastics and Composite Materials, Department of Polymer Engineering and Science, Montanuniversitaet Leoben, Otto Glöckel-Straße 2, Leoben, 8700, Austria
[6] Space Research Institute Graz, Austrian Academy of Sciences, Schmiedlstraße 6, Graz, 8042, Austria
[7] Department of Electronics and Nanotechnology, School of Electrical Engineering, Aalto University, Maarintie 8, Espoo, 02150, Finland
[8] University of Stuttgart, Pfaffenwaldring 29, Stuttgart, 70569, Germany
[9] Department of Aeronautics, Imperial College London, Exhibition Road, London, SW7 2AZ, United Kingdom
[10] Department of Physics, Umeå University, Umeå, Sweden
[11] Institute of Geophysics and Extraterrestrial Physics, Technische Universität Braunschweig, Braunschweig, 38106, Germany
[12] Faculty of Physics, University of Barcelona, Barcelona, 08028, Spain
[13] Institute of Physics/IGAM, University of Graz, Graz, Austria
[14] UMR8190 LATMOS (CNRS/Sorbonne Université), 4 place Jussieu, Paris, 75252, France
[15] UMR8109, LESIA, Observatoire de Paris, Université PSL, CNRS, Sorbonne Université, Université de Paris, 5 place Jules Janssen, Meudon, 92195, France
[16] Imperial College, London, United Kingdom
[17] Advanced Instrumentation for Nano-Analytics (AINA), Luxembourg Institute of Science and Technology, 41 Rue du Brill, Belvaux, 4422, Luxembourg
[18] Universitat Politècnica de Catalunya - BarcelonaTech (UPC), 11 Colom St., Terrassa, 08222, Catalonia, Spain
[19] University of Graz, Rechbauerstraße 12, Graz, 8010, Austria
[20] Department of Earth and Environmental Sciences, The University of Manchester, Manchester, M13 9PL, United Kingdom
[21] Faculty of Science, Technology and Medicine, University of Luxembourg, 2 Avenue de l'Université, Esch-sur-Alzette, 4365, Luxembourg
[22] Institute for Geophysics and Astrophysics, University of Graz, Graz, Austria
[23] Lulea University of Technology, Luleå, 97187, Sweden
[24] Space Research Laboratory, Centre for Energy Research, Konkoly-Thege Miklós út 29-33, Budapest, 1121, Hungary
[25] Laboratoire de Physique des Plasmas (LPP), CNRS, École Polytechnique, Sorbonne Université, Université Paris-Saclay, Observatoire de Paris, Palaiseau, 91120, France
[26] Dipartimento di Fisica "Enrico Fermi", Università di Pisa, Pisa, 56127, Italy
[27] University of Graz, Universitätsplatz 3, Graz, 8010, Austria
[28] Politehnica University of Bucharest, Bucharest, Romania
[29] Eidgenössische Technische Hochschule Zürich, Zürich, Switzerland
[30] Max–Planck-Institut für Sonnensystemforschung, Justus-von-Liebig Weg 3, Göttingen, 37077, Germany
[31] Vanderbilt University, 12201 West End Ave, Nashville, 37235, TN, USA
[32] The Center for Astrophysics, Harvard and Smithsonian, 60 Garden St, Cambridge, 02138, MA, USA
[33] LATMOS/IPSL, UVSQ Université Paris-Saclay, Sorbonne Universit, CNRS, Guyancourt, France

ARTICLE INFO

ABSTRACT

Induced magnetospheres form around planetary bodies with atmospheres through the interaction of the solar wind with their ionosphere. Induced magnetospheres are highly dependent on the solar wind conditions and

* Corresponding author.
  E-mail address: eva.kramer@umu.se (E. Krämer).

have only been studied with single spacecraft missions in the past. Without simultaneous measurements of solar wind variations and phenomena in the magnetosphere, establishing a link between both can only be done indirectly, using statistics over a large set of measurements. This gap in knowledge could be addressed by a multi-spacecraft plasma mission, optimized for studying global spatial and temporal variations in the magnetospheric system around Venus, which hosts the most prominent example of an induced magnetosphere in our solar system. The MVSE mission comprises four satellites, of which three are identical scientific spacecraft, carrying the same suite of instruments probing different regions of the induced magnetosphere and the solar wind simultaneously. The fourth spacecraft is the transfer vehicle which acts as a relay satellite for communications at Venus. In this way, changes in the solar wind conditions and extreme solar events can be observed, and their effects can be quantified as they propagate through the Venusian induced magnetosphere. Additionally, energy transfer in the Venusian induced magnetosphere can be investigated. The scientific payload includes instrumentation to measure the magnetic field, electric field, and ion–electron velocity distributions. This study presents the scientific motivation for the mission as well as requirements and the resulting mission design. Concretely, a mission timeline along with a complete spacecraft design, including mass, power, communication, propulsion and thermal budgets are given. This mission was initially conceived at the Alpbach Summer School 2022 and refined during a week-long study at ESA's Concurrent Design Facility in Redu, Belgium.

1. Introduction

Magnetospheres can generally be categorized in three main types. Those that arise due to the interaction of an intrinsic magnetic field (e.g. from a dynamo in Earth's case) with the solar wind, will henceforth be referred to as dynamo-generated magnetospheres. In the case of induced magnetospheres, where the parent body does not have an intrinsic field, the magnetosphere is created through the solar wind's interaction with the body's ionosphere. Examples of such induced magnetospheres are not only found around planets like Venus but around bodies such as comets [1] and moons [2] as well. The third composite type is a combination of an induced magnetosphere with remnant magnetic fields (such as Mars with its crustal magnetic fields). To fully understand magnetospheres and their dynamics, especially their dependence on solar wind conditions, all three types need to be studied. The intrinsic field type has already been extensively investigated [3], with Earth serving as a perfect laboratory (e.g. for the three prominent space plasma missions Cluster [4,5], THEMIS [6], and MMS [7]). Venus presents the ideal environment to study an induced magnetosphere as it does not possess remnant crustal fields contrary to Mars [8]. The study of such a system contributes to a fuller picture of magnetospheres, which has broad implications in the fields of comparative planetology. For instance, the similar size and density of Earth and Venus allow for a comparison between the two magnetospheric systems. Predictions could possibly be made about Earth's atmospheric evolution during pole reversal intervals, as the magnetic dipole moment diminishes and consequently the magnetosphere reduces in size [9]. As the interaction of a planet's magnetosphere with the solar wind has direct effects on atmospheric processes [10], insights into the planet's evolution can also be gained, which would also contribute to the study of exoplanets. Because laboratories on Earth fail to recreate similar conditions as in space, it is indispensable to use in-situ space measurements. The absence of disturbances at Venus (e.g. due to crustal fields) and its proximity to Earth makes it the optimal place to study induced magnetospheres.

The main regions of a dynamo-generated magnetosphere (e.g. bow shock, magnetotail etc.) are also present in an induced magnetosphere. However, due to the lack of an intrinsic magnetic field, all aspects of the induced system depend on the ionosphere and solar wind properties, such as particle density and bulk velocity, as well as the direction and strength of the interplanetary magnetic field (IMF). This makes the induced magnetosphere much more reactive, variable and unstable than a dynamo-generated magnetosphere. In planets with an ionosphere but no internal magnetic field, its interaction with the solar wind gives rise to a complex system of currents and electromagnetic fields. On the dayside, the currents result in a region of increased magnetic field, the induced magnetosphere boundary (IMB) [11]. The

direction of the current and the induced magnetic field is only dependent on the direction of the IMF. Any changes in the IMF orientation will therefore change the magnetic topology of the induced magnetosphere. This is not only the case for typical small variations during calm solar wind periods but especially during extreme solar events like interplanetary coronal mass ejections (ICMEs), corotating interaction regions (CIRs), and solar flares [12]. Strong disturbances in the solar wind parameters, such as an enhanced and smoothly rotated magnetic field, and a decreased proton temperature are typical characteristics of ICMEs [13]. CIRs are associated with coronal holes and form at boundaries between regions of slow and fast solar wind flow [14]. Solar flares can caused increased ionization in the ionosphere and can accelerate particles, which can enter the Venusian system. In summary, the key to understanding induced magnetospheres is linking the variations of the solar wind to changes in its structure and occurrence of dynamic processes.

The induced magnetosphere of Venus has been studied in the past by the dedicated missions Pioneer Venus Orbiter (PVO) (1978–1992) [15] and more recently Venus Express (VEX) (2006–2014) [16]. PVO had a suite of instruments for the measurement of electromagnetic fields and plasma properties. PVO's near-polar orbit was designed to cover scientifically interesting regions of the Venusian atmosphere and ionosphere on the dayside, to the far tail on the nightside. The VEX mission had a different orbit, which allowed the first observations of the near tail [17] and a unique study of the polar and terminator regions. It included plasma instruments as well, namely a magnetometer and a comprehensive plasma analyzer.

PVO was able to confirm the absence of a significant magnetic field. In addition, the presence of a bow shock, a magnetosheath, an induced magnetosphere boundary (IMB) as well as the induced magnetotail were reported [e.g. 18,19]. A sketch of Venus' induced magnetosphere is shown in Fig. 1. The bow shock has an average subsolar standoff distance of 1.36 R_V (Venus radius: 1 R_V = 6052 km) during the solar minimum and 1.46 R_V during the solar maximum [20]. The magnetic pile-up boundary is, similar to Earth's magnetopause, a region which separates the induced magnetosphere from the inner magnetosheath. Xu et al. [21] used VEX data to find the average location of the IMB during the solar maximum at 387 km. The extent of the Venusian magnetotail has been observed between $5 - 11$ R_V and the magnetic field polarity is dependent on the IMF [22].

These missions were altogether able to provide a comprehensive view of the plasma environment around Venus. However, they encountered limitations: both missions had limited time resolution of particle instruments, with PVO's measurement period at 10 min [23] and VEX's at 3 min for ions and 32 s for electrons [24]. For comparison, the MMS mission has a period below a second [25]. PVO and VEX were the only missions to investigate Venus' induced magnetosphere with dedicated plasma instruments. Their results are single point measurements, as both were only single spacecraft and operated in different
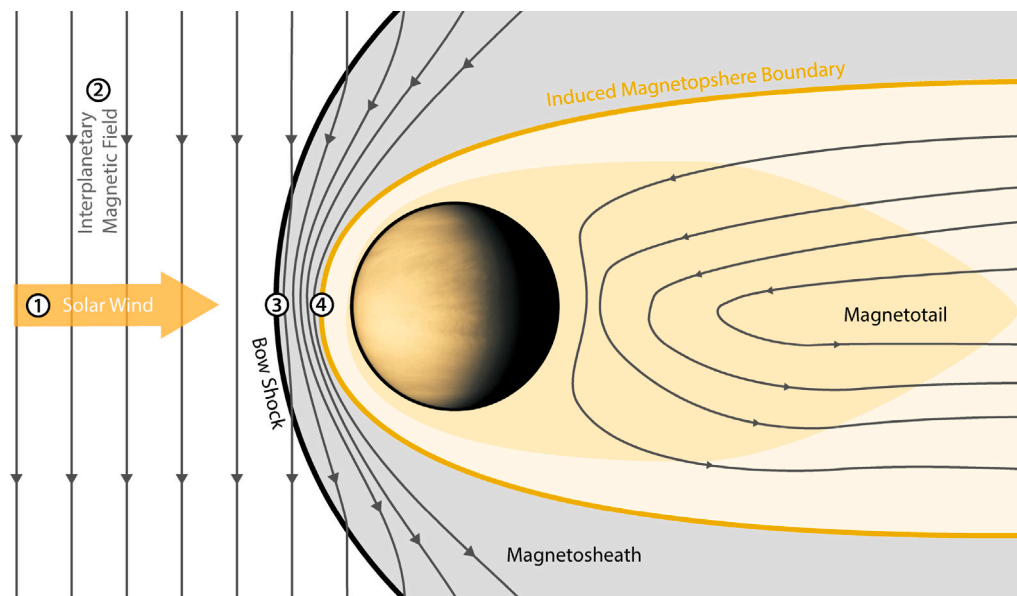
Fig. 1. Conceptual overview over the Venusian induced magnetosphere. The numbers indicate the different plasma regions: 1. the solar wind, 2. IMF, 3. Bow shock, 4. IMB.

orbits at different times. Establishing correlations between changes in the solar wind conditions and reactions of the magnetosphere with single-point measurements is only possible in special cases or with statistical methods relying on strong assumptions (i.e. slow variations of the solar wind). Vech et al. [26] studied the reaction time of the Venusian magnetosphere to polarity changes in the IMF, they found that the magnetospheric field rearranges itself within 10 min, while a reduction of the particle fluxes in the magnetotail was delayed by 2–8 h. This indicates a slower response of the ionosphere compared to the remaining magnetosphere. The study made use of orbits where the IMF significantly changed direction to correlate the reaction of the magnetosphere in the subsequent orbit. However, the authors lacked observations inside the magnetosphere during the polarity reversal to study the immediate response. A study by Slavin et al. [27] used VEX in combination with a flyby of Messenger and found that after 8.5 min a change in the IMF propagated from the position of Venus to 3 R_V tailwards along the Venus–Sun line. This study shows the importance of multipoint measurement to study the dynamics of an induced magnetosphere. In general, there is a lack of studies of global effects on induced magnetospheres caused by structural features in the solar wind. Thus, the overarching open question is how an induced magnetosphere reacts to variable solar wind conditions [17]. To study this question in detail, it is essential to monitor the upstream solar wind conditions simultaneously with the downstream measurements.

In Earth's magnetosphere, an important interaction process with the IMF is magnetic reconnection. It converts magnetic energy into kinetic energy through the rearrangement of the magnetic topology and acceleration of plasma. This process is frequently observed in the magnetotail and at the magnetopause, whenever the IMF and Earth's magnetic field form a so-called X-line. In induced magnetospheres the X-line can only be formed by the IMF, therefore reconnection is mainly expected to occur in the magnetotail, where the draped field lines meet [17]. Zhang et al. [28] found evidence of magnetic reconnection in the Venusian magnetotail, specifically, they observed plasma flow towards Venus with a magnetic field component transverse to the flow. Additionally, Dubinin et al. [29] found periodic outflow of planetary ions which which arised due to the flapping motion of the current sheet. The authors suggested that the flapping motion arises due to reconnection in the magnetotail which might contribute to the atmospheric loss at Venus. Rong et al. [30] suggested that the source of the flapping tail motion are perturbations in the magnetosheath flow rather than magnetic reconnection. Similar results were found by Kollmann

et al. [31] that studied fast plasma flows in the tail but could not find an increase occurrence rate close the neutral sheet which would be expected for reconnection events. This illustrates the need for further research to deduce the source of these fast flows and determine the importance of tail flapping and tail reconnection for the dynamics of the Venusian tail.

Waves in plasmas are also known to play an important role in the transfer and transport of energy. For example, in a collisionless plasma, waves transfer energy from one particle distribution to another or can accelerate particles to high energies. In order to understand the dynamics of a system, waves are a key element to transport information. Several waves have been identified at Venus [32] such as Whistler waves [33,34], Langmuir waves [34,35], mirror mode waves [36], and ion acoustic waves [33,34]. Yadav [32] suggested that Electron cyclotron waves, Ion cyclotron waves, and Mix-mode waves could also exist but they have not been observed yet. Wave detection in tandem with ion distribution measurements are useful tools to study waves as well as their effects and sources.

The bow shock can be divided into two regions depending on the angle θ_{Bn} between the bow shock normal and the IMF. When $\theta_{Bn} < 45°$ the bow shock is considered quasi-parallel, while $\theta_{Bn} > 45°$ is considered quasi-perpendicular. At the quasi-parallel bow shock, particles get reflected to the upstream region where they interact with the incoming solar wind which leads to instabilities and the growth of waves, constituting the foreshock region [37]. Due to the lack of an upstream monitor, the influence of the IMF direction on the induced magnetosphere is still not fully understood. Zhang et al. [38] reported the absence of the dayside induced magnetosphere during a period when the IMF was nearly aligned with the solar wind flow. This would correspond to a quasi-parallel subsolar bow shock. With the help of simulations the authors found that the IMF orientation has a significant impact on the atmospheric escape rate of Venus. Extreme solar wind conditions are rare at Venus but they can help our understanding of stellar wind interaction of stellar winds around very active stars and exoplanets [38].

A recent flyby by BepiColombo revealed a significant stagnation region in the dayside magnetosheath with an extent of 1900 km during a period of stable solar wind conditions [39]. The stagnation region is a subregion of the subsolar magnetosheath with a significantly reduced flow speed which limits the amount of energy transferred between the ionosphere and the solar wind. The region was only observed downstream of a quasi-perpendicular bow shock; the question remains

how this region is affected downstream of a quasi-parallel bow shock, e.g. through foreshock structures.

As mentioned before, the influence of extreme solar events (e.g. CIRs, ICMEs, solar flares) is vital for the dynamics of the Venusian induced magnetosphere [e.g. 40–42]. Edberg et al. [43] for example have found 147 CIR and ICME events in a 3.5 year interval during a solar minimum at Venus. Generally, during a solar maximum the number of extreme solar events can increase by an order of magnitude [44,45]. Due to the variable nature of these events, it is favorable to maximize the amount of observed extreme solar events, especially for statistical analysis.

The above mentioned examples show that while certain processes and phenomena are common to all magnetospheres, there are also some key differences that arise due to the presence or absence of an intrinsic magnetic field. Because the interaction of a planet's magnetosphere with the solar wind can have large-scale effects on its atmospheric evolution [17], the study of different types of magnetospheres is important in the context of understanding planetary systems. The benefit of a multi-spacecraft mission for the study of magnetospheric plasma physics has already been proven in several cases around the Earth. Here, we present such a multi-spacecraft mission concept for Venus that addresses the open scientific questions related to induced magnetospheres.

The Magnetospheric Venus Space Explorers (MVSE) mission investigates the dynamics of Venus' induced magnetosphere using three spin-stabilized science spacecraft and one three-axis stabilized communication spacecraft. The latter acts as a communication relay for the science spacecraft. The dynamics of Venus' plasma environment are highly dependent on the solar wind conditions, therefore necessitating the investigation of changes in plasma parameters in the dayside and nightside of the magnetosphere simultaneously. In addition, one needs to measure the variation in the solar wind. In order to obtain the three spacecraft in such a configuration as frequently as possible, it is necessary for the orbits to be synchronized.

The MVSE mission classifies as an L-class mission in Voyage 2050 program of the ESA science program. This proposed mission complements the currently planned ESA and NASA missions to Venus, namely DAVINCI [46], EnVision [47] and VERITAS [48]. Because these missions' objectives focus on the composition of Venus' atmosphere and the Venusian geology, they are not capable of answering the still open questions about Venus' magnetospheric environment even after the previous single-spacecraft plasma missions to Venus, namely VEX and PVO. A multi-spacecraft mission of the induced magnetosphere can provide the missing link to get a full understanding how Venus evolved over time and what role the solar wind interaction with the atmosphere played in Venus' past. Together they will provide a greater holistic view of Venus, from its interior up to its magnetosphere.

This paper is structured as follows; in Section 2 we present the scientific mission objectives and requirements, in Section 3 we present the scientific payload, in Section 4 we give an overview over the mission outline, and in Section 5 we present the system configuration of the mission.

2. Mission objectives and requirements

The overall goal for the MVSE mission is to understand dynamic processes in Venus' induced magnetosphere under the regular variations of the solar wind as well as during extreme solar events. This general target is further specified in form of three primary scientific questions:

- SQ1: How does the Venusian induced magnetosphere react to variations in the solar wind conditions?
- SQ2: How does the Venusian induced magnetosphere react to extreme solar events?
- SQ3: What processes transfer energy to the Venusian induced magnetosphere and how do they depend on varying solar wind conditions?

Table 1
Scientific objectives derived from the primary scientific questions of the MVSE mission.

	Scientific objective	Addresses question
SO1:	Monitor solar wind conditions.	SQ1, SQ2, SQ3
SO2:	Monitor spatial and temporal changes in the magnetospheric structure.	SQ1, SQ2
SO3:	Detect the effects of extreme solar events (e.g. flare, ICME and CIR)	SQ2
SO4:	Detect dynamic processes (e.g. waves in plasmas and transients)	SQ3

Table 2
Mission requirements grouped in three categories; mission requirements (MR), position requirements (PR) and timing requirements (TR) that follow from the objectives of Table 1.

From objectives		Mission requirement
All	MR1:	Measure the 3D magnetic field
All	MR2:	Measure the 3D electric field
All	MR3:	Measure the velocity distribution functions of the particles
SO4	MR4:	Measure the ion composition
SO1, SO3	PR1:	Probe undisturbed solar wind upstream of induced magnetosphere
SO2, SO4	PR2:	Probe the induced magnetosphere at two different locations
SO2, SO3	TR1:	Fulfill PR1 and PR2 simultaneously
SO3	TR2:	Perform measurements over a time period of minimum 2 years

These scientific questions allow for the definition of scientific objectives stated in Table 1. Accomplishing these objectives translates to a fulfillment of several requirements, which are grouped into three categories; measurement requirements (MR), position requirements (PR), and timing requirements (TR). From these requirements it becomes evident that the mission presupposes a multi-spacecraft concept, where a specific constellation has to be maintained (TR1). One spacecraft monitors the upstream solar wind, while the remaining two spacecraft detect the reaction of the induced magnetosphere at different locations. The remaining mission requirements are outlined in Table 2. Section 4 outlines a mission concept that optimizes the duration during which all requirements are fulfilled, while maintaining costs and complexity at a reasonable level.

The necessity to observe extreme solar events with an appropriate alignment of all three spacecraft puts an additional time constraint on the mission. For sufficient statistics, the mission shall observe at least 100 ICME events, therefore, requiring scientific operations over a two-year time period (TR2).

The scientific measurement requirements and instrument performances which follow from the objectives are listed in the following section.

3. Scientific payload

In the following, we give an overview of the proposed scientific payload which will be placed on each scientific spacecraft. We propose heritage instruments that are used to estimate the mass and energy consumption of our proposed payload. An overview of all instruments used, the number of instruments on each scientific spacecraft as well as the power, mass and data rate budget are given in Table 3.

3.1. Magnetometers (FGM/SCM)

The measurements of all vector components of the magnetic field are expected to occur in varying ranges. The magnetic field strength in the Venusian magnetosphere varies around $50 - 165$ nT [32] and

Table 3
Mass *m*, power *P* and data budgets for the scientific payload. The number *n* states how many instruments will be loaded on each scientific spacecraft.

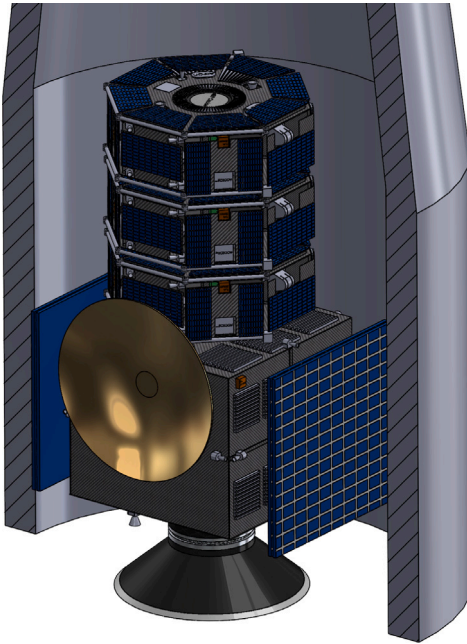| Instrument	n	m (kg)	P (W)	Data rate (kb/s)	Heritage instrument
FGM	2	0.29	1.49	0.15	THEMIS FGM [49]
SCM	1	0.46	0.27	1.3	MMS SCM [50]
SDP	4	4.3	0.34	0.75	BepiColombo MEFISTO [51]
ADP	2	3.18	2.3	0.75	MMS ADP [52]
ESA	2	1.6	2.25	6	THEMIS ESA [53]
MSA	1	4.46	8.2	10	BepiColombo MSA [54]
HEP	1	1.98	7.84	2.26	BepiColombo HEP [55]
ASPOC	2	2.9	3.5	0.1	MMS ASPOC [56]
Total		40	47	31	

Fig. 2. Scheme of the stacked configuration inside the Ariane's fairing.

is generally lower in interplanetary space. Furthermore, the ability to detect low and high-frequency electromagnetic waves is essential, as waves are known to contribute to energy transfer processes in the magnetosphere as explained in detail in Section 1.

In this regard, fluxgate and search coil magnetometers are highly reliable and long-proven instruments that safely fulfill all requirements. For the former, the THEMIS fluxgate magnetometer (FGM) serves as a Ref. [49]. It covers a sufficiently large field strength range. The time resolution is 128 Hz, which allows the detection of waves with frequencies up to 64 Hz. For high-frequency waves, the MMS search coil magnetometer (SCM) [50] is proposed, which measures magnetic fluctuations with frequencies between 1 Hz–6 kHz.

3.2. Electric field probes (SDP/ADP)

A commonly used method for the 3D measurement of static and varying electric fields in space is the double probe technique [57]. As in previous comparable space missions (Cluster, THEMIS and MMS), the usage of two pairs of spin plane double probes (SDP) and one pair of axial double probes (ADP) is proposed. The tip to tip distance of the SDP is 31.6 m, with a wire boom length of 15 m. For theSDP, Bepi-Colombo Mercury Electric Field In-Situ Tool (MEFISTO) [51] serves as a reference. It can measure static and variable electric fields with frequencies up to 10 MHz. As the deployment of this instrument requires

a spinning spacecraft, it is also one of the main design drivers for the main system architecture.

For the ADP, we propose the usage of probes with heritage from the one onboard MMS [52]. The instrument provides electric field measurements for DC to 100 kHz with a tip-to-tip distance of 31.6 m.

3.3. Electrostatic analyzer (ESA)

The mission will measure both ion and electron velocity distributions. These distributions will be measured by two top-hat electrostatic analyzers (ESAs). We propose the THEMIS ESA instrument as heritage [53]. It provides electron distributions over the energy range 2 eV up to 32 keV and ion distributions from 1.6 eV to 25 keV. The instrument covers a full solid angle over each 4 s spin-period. It provides measurements in 31 energy bins with a resolution of $\Delta E/E \sim 32\%$. The resolution in the rotation phase is 11.25 deg and in the polar angle is 22.5 deg for the electron sensor. The resolution in the polar angle is up to 5.625 deg for the ion sensor close to spin plane. The ion resolution decreases closer to the spin axis. This allows the instrument to resolve solar wind ions. The electrostatic analyzers are another key driver for the spin-stabilized scientific spacecraft. A spin-stabilized spacecraft allows a 4π solid angle coverage of the electron and ion distributions.

3.4. High energy particle instrument (HEP)

The detection of extreme solar events, for example CMEs and solar flares, requires the detection of high-energy electrons and ions. Therefore, a high-energy particle instrument will be used with heritage from BepiColombo's high-energy particle instrument (HEP) [55]. The instrument has two sensors to detect both electrons and ions. The electron sensor can detect particles from $30 - 700$ keV, while the ion sensor detects particles from $30 - 1500$ keV. Both sensors have a time resolution of 4 s.

3.5. Mass spectrometer (MSA)

In addition, the mission will utilize a mass spectrometer to resolve different species of ions. We propose the mass spectrometer (MSA) on board BepiColombo's MMO spacecraft [54]. The instrument has a time resolution of one spin (4 s), and can resolve energies between 1 eV/q - 38 keV/q and masses between $1 - 60$ amu. The field of view of the MSA is 4π [58].

3.6. Active spacecraft potential control (ASPOC)

In order to improve the particle measurements and electric field measurements we propose an active spacecraft potential control to reduce the spacecraft's electric potential. As heritage, the Active Spacecraft Potential Control (ASPOC) on the MMS mission can be utilized [56]. It keeps the spacecraft potential below 4 V by emitting indium ion beams.

4. Mission outline

The mission consists of three science spacecraft (SSC) which perform all required measurements and a transfer vehicle (TV), which provides propulsion for the transfer, and is then used for communications. These spacecraft are stacked on top of each other and thus the launch assembly is called the spacecraft stack. A representative scheme of the stack is presented in Fig. 2. Table 4 shows the mass budget for the individual spacecraft as well as the complete stack. Section 5 provides a detailed description of the spacecraft. The final orbits of the spacecraft are depicted in Fig. 3. Two SSC will be placed in a circular orbit with 180° phase difference and an orbital period of 20 h. The third SSC will be placed in an elliptical orbit. The TV is placed in the same circular orbit as the SSC with a 90° phase shift. The total Δv required to get the SSC and TV into their final orbits is 2015 m/s.

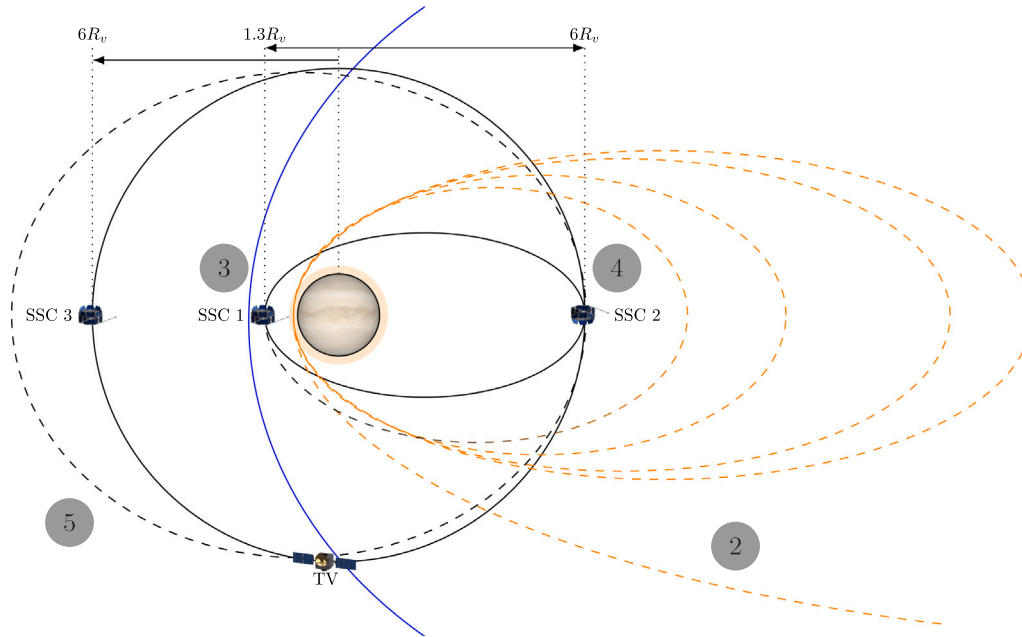The transfer can be broken down into five phases:

Fig. 3. Mission phases at Venus as described in Section 4.

Table 4
Mass budgets for science satellite (dry), transfer vehicle (dry) and spacecraft stack (wet).

Science spacecraft (SSC)		Transfer vehicle (TV)	
Subsystem mass	[kg]	Subsystem mass	[kg]
AOCS	30.5	AOCS	67.1
Instruments+Electronics	60.7	Propulsion	157.0
Mechanisms	36.9	Mechanisms	13.2
Power	83.1	Power	102.4
TT&C	25.6	TT&C	45
Structure	104.5	Structure	352.1
Thermal	11.6	Thermal	26.4
Harnesses	17.7	Harnesses	38.2
20% margin	74.5	20% margin	160.3
Total	448.1	Total	961.7

Spacecraft stack	
Unit	Mass incl. margin
Science Spacecraft #1	448 kg
Science Spacecraft #2	448 kg
Science Spacecraft #3	448 kg
Transfer Vehicle (incl. propellant)	2831 kg
Launch Adapter A64	120 kg
Total	4295 kg

0. Escape and interplanetary transfer The escape was modeled using the Ariane 64 to insert the spacecraft stack into an elliptical interplanetary trajectory to Venus (Hohmann-type manoeuvre). A 3 week launch window is selected around 2032-12-06, for an arrival at Venus 6 months later.

1. Minor interplanetary correction 15 days after launch a small correction manoeuvre is necessary to place the spacecraft stack at the desired pericythe from Venus.

2. Orbit insertion and aerobraking 157 days after launch, a capture manoeuver is performed at a pericenter height of 900 km from Venus' surface. In order to lower the apocythe sufficiently after capture, aerobraking is convenient to keep the required propellant within feasible quantities. This phase lasts one year.

3. Elliptical science orbit Once aerobraking is completed, the pericythe is raised to achieve an elliptical orbit with a pericythe of $r_p = 6952$ km ($1.3R_v$) and an apocythe of $r_a = 24052$ km ($6R_v$), as seen in Fig. 3. At this point the first science spacecraft (SSC) is detached from the spacecraft stack.

4. Circularization At the apocythe of the elliptical orbit an impulsive manoeuvre is performed to place the spacecraft stack of two remaining SSC and the TV into a large circular orbit, with $r_a = r_p = 24052$ km ($6R_v$), as shown in Fig. 3. The second SSC is released in this new orbit.

5. Minor Phasing manoeuvres In the circular orbit a small manoeuvre is performed to lower the semi-major axis, just after the second SSC is detached. The spacecraft stack of the third science satellite and the TV is moved into an elliptical orbit, whose period is shorter and is a multiple of the period of the circular orbit. After a few revolutions a phase displacement of π is achieved and the same impulsive manoeuvre is performed to return to the circular orbit. The third SSC is released with a 180° phase shift to the second SSC. The same is performed for the TV, but in this case the phase angle is smaller without a strict constraint.

A time of the events and their location is shown in Table 5.

5. System configuration

5.1. Spacecraft architecture and structure

The architecture of the four spacecraft involved in the MVSE mission is conditioned by the distribution of functionalities among them. Namely, the three scientific spacecraft perform in-situ plasma measurements, and therefore their design has been optimized to fully utilize their payload capabilities. The technical solution adopted for the spacecraft is a spin-stabilized octagonal design, due to the following considerations:

- To provide complete 360° coverage of the azimuthal plane to any payload probe pointed radially outwards.

Table 5
Mission timeline including dates of most important mission events.

	Days from launch	Event	Location
1.	0	Direct interplanetary insertion	Kourou
2.	158	Venus capture	Highly elliptical orbit
3.	523	Aerobraking completed	Elliptical orbit
4.	523	Pericytherion raise	Elliptical science orbit
5.	523 + x	Deposit science s/c 1	Elliptical science orbit
6.	523 + x	Circularization	Circular science orbit
7.	523 + x	Deposit science s/c 2	Circular science orbit
8.	523 + x	Phasing manoeuvre	Circular science orbit + 180 deg
9.	523 + x	Deposit science s/c 3	Circular science orbit + 180 deg
10.	523 + x	Phasing manoeuvre	Circular science orbit + 270 deg
11.	523 + x	Communications s/c in position	Circular science orbit + 270 deg
12.	523 + 2 yrs	End of mission	

(a)

(b)
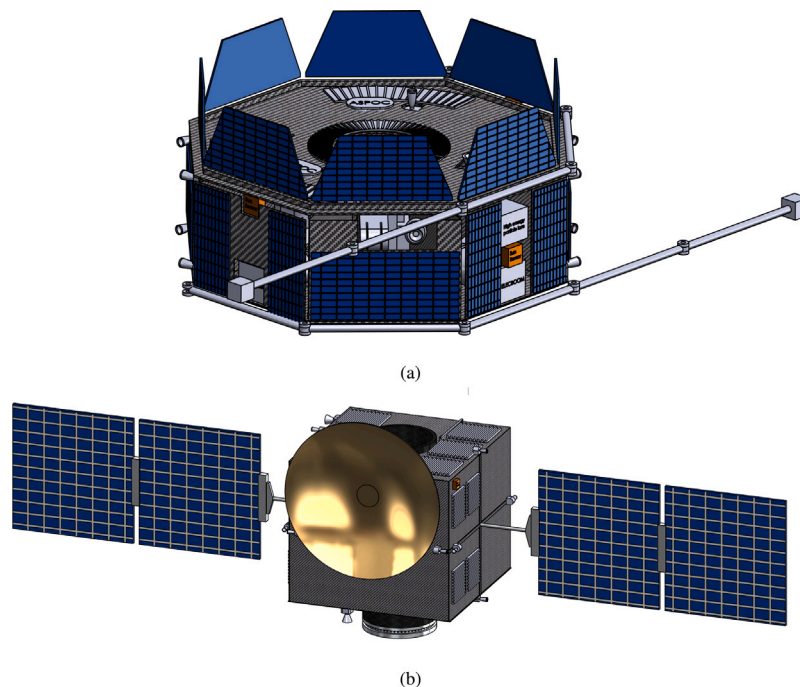
Fig. 4. Spacecrafts in the deployed configuration (not to scale). (a) Scientific spacecraft. (b) Transfer vehicle structure. The wire booms of the Scientific spacecraft were omitted for clarity reasons.

• To enable inertial deployment of long-distance wire booms.

The octagonal layout allows achieving a cylinder-rotor inertia that maintains the spinning axis perpendicular to the ecliptic plane.

The fourth spacecraft provides the functionality of a propulsive transfer stage in the interplanetary trajectory to Venus. After the orbit insertion of the three scientific spacecraft, the transfer stage remains orbiting Venus as a communications relay. The proposed technical solution is a prismatic, three-axis-stabilized spacecraft. Independent stabilization is required to enable precise pointing of the high-gain antenna with the ground communications segment back on Earth. Concurrently, the prismatic shape provides the necessary inner volume to allocate all the necessary components and payload, while offering a wide lateral surface to anchor the high-gain antenna. Both types of spacecraft are depicted in the schematics presented in Fig. 4.

In adherence to the spin-stabilized configuration, a cylindrical central core that aligns with the spinning axis of the spacecraft was implemented. This core acts as the primary structural component, allowing for the stacking of the science spacecraft and incorporation of propellant tanks, resulting in smoother load transfer during the various mission phases. The spacecraft also incorporates shear panels connected to the bottom, top, and side panels, increasing their rigidity and stability. The chosen material for the primary structures is an aluminum honeycomb sandwich structure with Carbon-Fiber-Reinforced Polymer

(CFRP) face sheets, providing necessary stiffness to withstand launch loads, and proven to be a reliable material structure for spacecraft due to its multifunctional properties, including low outgassing rates, low coefficient of thermal expansion (CTE), low weight, and high strength [59,60].

The transfer vehicle features dimensions of $2.0\,\text{m} \times 2.0\,\text{m} \times 2.2\,\text{m}$, whereas the scientific spacecraft have a diameter of $2.0\,\text{m}$ and a height of $0.7\,\text{m}$. The central cylindrical core used in both spacecraft types has a diameter of $0.9\,\text{m}$. The general arrangement of the structure is shown in Fig. 5(a) for the scientific spacecraft and Fig. 5(b) for the transfer vehicle. Both the structural and material concepts exhibit a high level of technology readiness and draw upon heritage from previous missions such as LISA pathfinder [61,62], Dawn [63], and MAVEN [64].

5.2. Attitude and orbit control

In the context of this mission, the purpose and design of the Attitude and Orbit Control Subsystem (AOCS) is dictated by the requirements of the science instrumentation payload as well as the other spacecraft systems. The communications strategy employed, requires that the transfer vehicle be able to orient its antenna to precisely track each of the science satellites as well as Earth, hence 3-axis-stabilization was implemented. Since the instrument payload requires a baseline spin
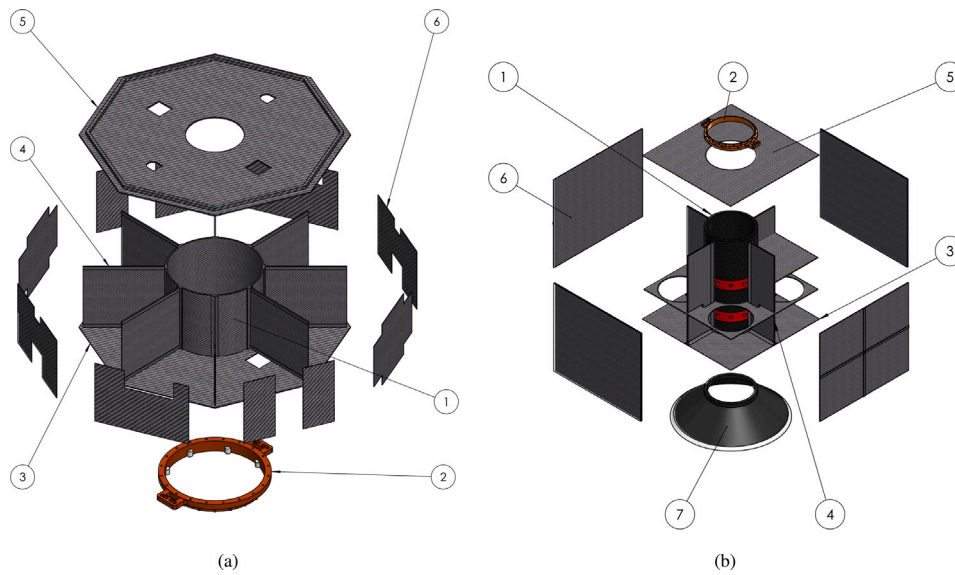
Fig. 5. Structure of both spacecraft types (not to scale). (a) Scientific spacecraft structure. (b) Transfer vehicle structure. Legend: (1) Central core, (2) Satellite separation ring, (3) Bottom panel, (4) Shear panel, (5) Top panel, (6) Side panel and (7) Payload adapter.

Table 6
Breakdown of AOCS operations and thruster propellant mass requirements.

Operation	Propellant consumed (kg)	No. ops. expected	Total mass rqd. (kg)
SSC (Spin up/down)	0.167	8	1.3
SSC (De-tumble)	0.005	170	0.8
TV (BBQ mode)	0.050	4	0.2
TV (Aero-braking)	0.301	100	30.1
TV (Communications)	0.001	852	0.8
TV (De-tumble)	0.167	852	21.7

rate of 15 rpm to ensure adequate field of view and temporal resolution for data collection and the science satellite spin plane needs to be aligned with the ecliptic, a spin-stabilized approach was chosen to take advantage of the gyroscopic effect to dampen attitude perturbations and to minimize the severity of disruption to science data collection in the event of failure of the AOCS actuators or running out of thruster propellant.

Loss of attitude control for any given satellite is sufficient to compromise science data collection hence redundancy of systems is paramount in AOCS design. Each science satellite in addition to the transit vehicle features its own AOCS suite, enabling necessary attitude and orbit corrections to be performed at an individual level. In the initial stages of the mission where the spacecraft are still combined these systems can be coordinated and actuated together to exert greater maneuvering authority over the spacecraft ensemble. From a sensors perspective, the suite for each satellite is composed of 3 star trackers, 4 sun sensors and 2 inertial measurement units (IMUs) to obtain complete attitude determination with redundant elements. 12 thruster blocks (each featuring 2 nozzles in cold redundancy) are incorporated to enable full 6 degree-of-freedom movement. These are cold gas monopropellant thrusters which draw propellant from separate tanks and piping from the propulsion system. The propellant considered for the AOCS during this study was hydrazine given its high specific impulse, ability to handle multiple cold restarts and extensive flight heritage, including the ARIEL science mission currently in development. The transfer satellite also features 4 reaction wheels in a tetrahedron configuration for fine rotation control.

Table 6 summarizes the main operations that the AOCS performs over the mission duration and the corresponding AOCS thruster propellant consumption. A 2% margin was added to the total required AOCS propellant mass for each spacecraft to account for propellant residuals. During transit to Venus, the spacecraft stack is slowly rotated along

its longitudinal axis, evenly distributing the thermal loads from the sun. This is commonly known as a "barbecue roll" or "BBQ mode", as referred to in Table 6. This maneuver must be started and ended using the AOCS thrusters. The aero-braking phase that occurs during insertion in Venus orbit requires a significant portion of the allocated thruster propellant budget due to both the strong aerodynamic forces encountered while in the upper parts of the Venusian atmosphere which induce large rotation rates combined with the larger moment of inertia of the spacecraft in transit configuration, requiring extended AOCS thruster burns to maintain constant attitude. During communications mode the transfer vehicle is expected to be able to slew at a rate of up to 1 °/s as it changes which target it is tracking. Tracking is performed exclusively with the reaction wheels to meet the 0.3° pointing accuracy for the high-gain antenna. Orbit control becomes prominent once the satellites have been inserted into their operational orbits around Venus. As a worst case scenario, it was assumed that the SSC need to perform orbital corrections every 10th orbit, requiring a de-spin and spin-up.

The AOCS of each satellite was sized to be able to recover from multi-axis tumbles of up to 3.5 °/s, which each of these recovery manoeuvres expecting to last up to a maximum of 30 s. Considered sources for these tumbles include satellite decoupling, thruster actuator failure and orbital perturbations. The transfer satellite is sized up to recover from tumbles while it is docked to the other satellites during transit. A pessimistic approach assumes frequent de-tumbling required every few orbits, with the expectation that the oversized AOCS propellant budget shown in Table 6 will allow for further mission extension.

5.3. Propulsion

The propulsion subsystem is part of the transfer module and shall deliver the TV (962 kg dry mass) and the scientific s/c (3 × 448 kg wet mass) from an interplanetary trajectory to their respective target orbits around Venus.

A trade-off study showed that chemical propulsion is advantageous over solar electric propulsion (EP). The reasons for this are the faster transfer and the resulting lower operating costs. Especially in view of the inevitably cost-intensive launch with an Ariane 64, low operating costs are desirable. Even with the electric propulsion (EP) option, the maximum launch mass of Ariane 62 is exceeded. The high specific impulse of the regarded EP systems and the high availability of solar power are revoked by the greater Δv demands (>10 000 m/s) of the EP

Table 7

Chemical propellant demands originating from the six maneuvers carried out by the transfer stage. The mission phases refer to Table 5.

Maneuver	Δv (m/s)	Propellant mass (kg)	Mission phase
Interplanetary correction	30	40	1.
Venusian orbit insertion	640	760	2.
Pericythe raise	181	188	4.
Circularization	1155	835	6.
Phasing	10	4.5	8./10.
EOL	10.5	3.2	12.
Total	2026	1831	
Total incl. 2% margin		1867	

Table 8

Data transfer rates and downlink times between the spacecraft and the ground station.

Direction	Data rate		Downlink time	
	Min.	Max.	Min.	Max.
SSC (circular orbit) ↔ TV	300 kbps	300 kbps	1.3 h	1.3 h
SSC (elliptical orbit) ↔ TV	140 kbps	>2.3 Mbps	<10 min	>2.5 h
TV → Earth	180 kbps	8.0 Mbps	8.5 min	6.3 h

Table 9

Total instrument and subsystem data rates of the spacecraft.

Direction	Max.	Duty cycle	Mean
Nominal science mode	38.3 kbps	24 %	9.2 kbps
Burst mode	662.2 kbps	1 %	6.6 kbps
Total	–	–	15.8 kbps

option. This is a manyfold increase in the Δv requirement of the chemical alternative, which is significantly lowered by 988 m/s to 2026 m/s by aerobraking in the Venusian atmosphere. (this paragraph was moved a bit up)

The selected engine is the LEROS 4 Interplanetary Engine (Nammo Space, UK), which will also be used in ESA's EnVision mission to Venus [65]. The engine uses MON-3/MMH bipropellant and has a specific impulse of 318 s. The Δv budget from STK trajectory simulations together with the estimated dry mass of the TV and wet masses of the science spacecraft yield a required propellant mass of 1867 kg (including margins). The total wet mass of the spacecraft stack thus amounts to 4174 kg.

Table 7 summarizes the simulated Δv budgets for the mission maneuvers and the required propellant masses. For the interplanetary correction an absolute margin of 30 m/s was considered. For the Venus orbit insertion and end of mission we considered a 10 m/s margin. The margin for the end of the mission was added to raise the spacecraft to a graveyard orbit. All maneuvers expect the interplanetary correction a 5% relative Δv was added. Finally, there is 2% margin on the Propellant mass.

Besides the LEROS 4 Interplanetary Engine, the propulsion subsystem entails one fuel tank (MMH), one oxidizer tank (MON-3) and two pressurant tanks (Helium) to ensure reliable discharging of the tanks. Propellant pipes and valves are also factored into the mass calculation. This leads to a propulsion system dry mass of 157 kg. For the valves, an active power consumption of 200 W with a duty cycle <0.01 was assumed.

Further conceptualization work assessed several possible scenarios for off-nominal propulsion system events that could pose a risk to the overall mission. These scenarios include single-point failure of a sole thruster, implementation of off-nominal thrust and deviation from nominal target attitude during thrust which might end in deployment in off-nominal orbits. In addition, scenarios of fuel leakage and deviations of the fuel from the nominal temperature and pressure range were taken into account. To cope with these, margins have been included. It should be noted that further margins have already been factored in the Δv budget given in Table 7.

5.4. Communication

Given the large distance between Venus and Earth, a communication system with high transmission power, as well as antenna pointing precision and accuracy, is required. To reduce the combined complexity and mass of the spacecraft, only the transfer vehicle is equipped with the ability to efficiently communicate with Earth. The transfer vehicle carries a 2.0 m diameter, high-gain dish antenna that is rigidly mounted to the main spacecraft structure. The transfer vehicle AOCS is responsible for achieving and maintaining the pointing required for successful communication between the transfer vehicle and Earth. For low data rate emergency communications, the transfer vehicle carries a dipole antenna.

The high-gain antenna of the transfer vehicle is also required for communication within the mission constellation. The science spacecraft, on the other hand, employ hot-redundant dipole antennas, which allows for less strict pointing requirements for the science spacecraft. For example, it is sufficient that the science spacecraft are orbiting Venus and rotating around their own spin axis in roughly the same plane as the transfer vehicle. The science spacecraft must, one at a time, regularly offload their data to the transfer vehicle that can subsequently downlink the data back to Earth. They do so using a "burst" mode outside the scientifically relevant sections of the orbit. The transfer vehicle is responsible for initiating data transfer with the science vehicles. During the transit to Venus the BBQ rolling maneuver will be interrupted occasionally in order to test communication between the transfer vehicle and the ground stations.

Link budget analysis shows that sufficient data rates between the spacecraft can be achieved without directional antennas on the science spacecraft. The data transfer rates achieved during mission operations at Venus are detailed in Table 8. From the downlink rates and the instrument data rates shown in Table 9, the best and worst case data downlink times between the spacecraft and Earth have been calculated, and are presented in Table 8. The downlink time estimations show that downlinking all the data produced during the mission is feasible.

5.5. Power

Assessing the power budget of spacecraft involves studying their operational modes to identify the most power-demanding configuration. Power consumption is at its highest peak in Communication Mode for both spacecraft types. This power demand is attributed to the substantial energy utilization during the downlink phase. This mode's power consumption is the one chosen to guide the sizing of the solar panels and the batteries.

For the transfer vehicle, modes range between 1102.7 W to 85.5 W. The latter is reached at the beginning of the mission in Launch Mode, where power is sustained in an idle state. Additionally, the Safe Mode is employed when power conservation is prioritized for battery charging. Detailed values for each mode are available in Table 10.

The science vehicle has more operational modes than the transfer vehicle, as it operates with Science Mode, where payload instruments consume the most power. An extra state, namely Burst Science Mode, is introduced to address instances of heightened activity when the payload operates at its peak. Details can be found in Table 10.

Solar panels with Triple Junction III–V technology will be used for the spacecraft, providing a high power density of 38 W/kg, an efficiency of 29.5%, with a beginning of life (BOL) power capability of 616, 7 W/m^2 and an end of life (EOL) power capability of 522, 2 W/m^2. The transfer vehicle requires two deployable solar panels with a size of 3.99 m^2 and a mass of 8.23 kg each. The science spacecraft requires 8 fixed panels 0.55 m^2 in size with a mass of 1.2 kg each.

Table 10
Power consumption of both spacecraft in different operational modes. Highlighted the most demanding mode in sunlight: Communication. Also shown is Safe Mode which the spacecraft will enter in case of low power availability. A margin of 20% must be applied for all values.

Transfer vehicle	[W]	Science spacecraft	[W]
Comms	1102.7	Comms	490.8
Launch	87.5	Launch	85.7
Cruise	383.7	Cruise	206.0
Maneuver	668.28	Maneuver	307.2
Comms eclipse	517.7	Science	283.5
Safe	650.9	Science burst	289.7
		ISL eclipse	490.8
		Safe	226.4

The chosen secondary source is Nickel–Cadmium batteries. This type was chosen due to a wide temperature range of 45 °C to −20 °C, and the high number of cycles that it takes to reach 25% depth of discharge. The transfer vehicle requires a battery with a volume of $0.011\,\text{m}^3$ and mass of $34.07\,\text{kg}$, while the science spacecraft requires a battery with a volume of $0.0085\,\text{m}^3$ and mass of $32.25\,\text{kg}$.

5.6. Thermal

The thermal control design is based on the temperature constraints of internal components and the external radiating sources, taking into account both hot (at the orbit's perigee and when facing the Sun) and cold (during orbit's eclipse and interplanetary transfer) cases. The equilibrium temperature of both TV and SSC has been evaluated through a one node analysis. In this case, the thermal sources are the Sun, Venus' albedo and infrared radiation, and dissipated power. The incident power will balance with the radiating one, determined by the emitted power under the assumption of a uniform gray body: $\alpha_{vs}S_f A_{sun} + a\alpha_{vs}S_f A_{sun} + 0.5\alpha_{ir}S_f A_{sun} = \epsilon_{ir}\sigma T_{eq}^4 A_{tot}$. In the equation, σ is the Stephan–Boltzmann constant, T_{eq} is the equilibrium temperature of the spacecraft, A_{tot} is the total surface of the spacecraft, A_{sun} is the area of the spacecraft exposed to the Sun, a is Venus' albedo, assumed to be 0.7, S_f is the solar flux, α_{vs} is the absorbance in the visible spectra, α_{ir} is the absorbance in the infrared spectra and ϵ_{ir} is the emissivity in the infrared spectra. We assumed that the spacecraft is a gray body, $\alpha_{ir} = \epsilon_{ir}$. The emissivity and absorbance are considered as a weighted mean between respectively the emissivity and the absorbance of the materials used on the surfaces. For the SSC an average emissivity $\bar{\epsilon}$ of 0.605 and an average absorbance $\bar{\alpha}$ of 0.62 were assumed. For the TV $\bar{\epsilon} = 0.59$ and $\bar{\alpha} = 0.57$ were assumed. This emissivities are also used for sizing the radiators. To ensure an internal temperature of about 10 °C, the following solutions have been implemented:

- Radiators are placed on the sides of the spacecraft. Their total surface area is $2.865\,\text{m}^2$ for the SSC, and $3.574\,\text{m}^2$ for the TV.
- Silver multi-layer-insulation is used on the exposed areas not covered by solar panels with a thickness of $1.6\,\text{mm}$. For this material it has been assumed an emissivity ϵ of 0.02 and an absorbance α of 0.07.
- Internal electric heaters are only present in the transfer vehicle and require a total power of $172.9\,\text{W}$.

6. Conclusion

We have presented a multi-spacecraft mission to Venus to study the dynamics of induced magnetosphere called MVSE. Its aim is to provide the first in-situ measurements of an induced magnetosphere and its dynamics for at least 2 years. Continuous measurement will be made when at least two spacecraft are located inside the induced magnetosphere which will be the case 40–50% of the orbit time.

Such measurements will enhance general understanding of how the Sun drives the dynamics of an induced magnetosphere, contribute to a better understanding of planetary evolution and Earth's plasma environment when the magnetic field is weakened. Measurements will be taken simultaneously in the pristine solar wind and different regions in the induced magnetosphere of Venus. Three identical spin-stabilized science spacecrafts are baselined to facilitate these measurements, with an additional transfer vehicle acting as a communication relay. The instruments aboard the scientific spacecraft facilitate high precision 3D measurements of the electric field, magnetic field, as well as measuring the particle distribution functions and ion composition. The satellite constellation and scientific payload will enable us to record changes in the solar wind and how they affect the magnetosphere. Preliminary engineering studies show that this mission concept is feasible with current technology, building on previously flown instrumentation and presenting a possible trajectory sequence. The overall launch mass of 4350 kg requires a heavy launcher and the mission would classify as a L-class mission in the ESA's Voyage 2050 campaign. Should further work show a need for descoping, the axial double probes could be removed, decreasing the accuracy of the 3D electric field measurements. If a careful calibration of the ion and electron measurements can be achieved, the ASPOC may also be omitted.

Overall, this proposal demonstrates a technically feasible solution for the study of induced magnetospheres with a multi-spacecraft plasma mission. The scientific return from such a mission is expected to not only improve knowledge in the field of space plasma physics but also in general planetology.

Declaration of competing interest

The authors declare that they have no known competing financial interests or personal relationships that could have appeared to influence the work reported in this paper.

References

[1] T. Cravens, T. Gombosi, Cometary magnetospheres: a tutorial, Adv. Space Res. 33 (11) (2004) 1968–1976.

[2] M.G. Kivelson, Moon–magnetosphere interactions: a tutorial, Adv. Space Res. 33 (11) (2004) 2061–2077.

[3] D.J. Southwood, A brief history of the magnetosphere, in: Magnetospheres in the Solar System, American Geophysical Union (AGU), 2021, pp. 1–13, http://dx.doi.org/10.1002/9781119815624.ch1, URL https://agupubs.onlinelibrary.wiley.com/doi/abs/10.1002/9781119815624.ch1.

[4] C. Escoubet, R. Schmidt, M. Goldstein, Cluster - Science and mission overview, Space Sci. Rev. 79 (1) (1997) 11–32, http://dx.doi.org/10.1023/a:1004923124586.

[5] S. Hajra, N. Dashora, J. Solomon Ivan, On the multi-scale dynamics and energy flow near reconnection regions in the magnetopause and magnetotail using the MMS, cluster and THEMIS observations during the geomagnetic storm of 31 December 2015, Adv. Space Res. 72 (8) (2023) 3229–3250, http://dx.doi.org/10.1016/j.asr.2023.06.025, URL https://www.sciencedirect.com/science/article/pii/S0273117723004635.

[6] J.L. Burch, V. Angelopoulos (Eds.), The THEMIS Mission, Springer New York, 2009, http://dx.doi.org/10.1007/978-0-387-89820-9.

[7] S.A. Fuselier, W.S. Lewis, C. Schiff, R. Ergun, J.L. Burch, S.M. Petrinec, K.J. Trattner, Magnetospheric multiscale science mission profile and operations, Space Sci. Rev. 199 (1–4) (2014) 77–103, http://dx.doi.org/10.1007/s11214-014-0087-x.

[8] J.S. Halekas, J.G. Luhmann, E. Dubinin, Y. Ma, Induced magnetospheres, in: Magnetospheres in the Solar System, American Geophysical Union (AGU), 2021, pp. 391–406, http://dx.doi.org/10.1002/9781119815624.ch25, URL https://agupubs.onlinelibrary.wiley.com/doi/abs/10.1002/9781119815624.ch25.

[9] J.A. Caggiano, C.S. Paty, Analysis of e × b drifts in earth's magnetosphere during geomagnetic reversals: Potential consequences for plasmasphere behavior and stability, J. Geophys. Res. Space Phys. 127 (2) (2022) e2021JA029414, http://dx.doi.org/10.1029/2021JA029414, URL https://agupubs.onlinelibrary.wiley.com/doi/abs/10.1029/2021JA029414.

[10] G. Gronoff, P. Arras, S. Baraka, J.M. Bell, G. Cessateur, O. Cohen, S.M. Curry, J.J. Drake, M. Elrod, J. Erwin, K. Garcia-Sage, C. Garraffo, A. Glocer, N.G. Heavens, K. Lovato, R. Maggiolo, C.D. Parkinson, C. Simon Wedlund, D.R. Weimer, W.B. Moore, Atmospheric escape processes and planetary atmospheric evolution, J. Geophys. Res. Space Phys. 125 (8) (2020) e2019JA027639, http://dx.doi.org/10.1029/2019JA027639, URL https://agupubs.onlinelibrary.wiley.com/doi/abs/10.1029/2019JA027639.

[11] C. Bertucci, C. Mazelle, M.H. Acuña, C.T. Russell, J.A. Slavin, Structure of the magnetic pileup boundary at Mars and Venus, J. Geophys. Res. Space Phys. 110 (A1) (2005) http://dx.doi.org/10.1029/2004JA010592, arXiv:https://agupubs.onlinelibrary.wiley.com/doi/pdf/10.1029/2004JA010592, URL https://agupubs.onlinelibrary.wiley.com/doi/abs/10.1029/2004JA010592.

[12] D.A. Brain, Induced magnetospheres, in: Magnetospheres in the Solar System, American Geophysical Union (AGU), 2021, pp. 441–451, http://dx.doi.org/10.1002/9781119815624.ch28, URL https://agupubs.onlinelibrary.wiley.com/doi/abs/10.1002/9781119815624.ch28.

[13] L. Burlaga, E. Sittler, F. Mariani, a.R. Schwenn, Magnetic loop behind an interplanetary shock: Voyager, helios, and IMP 8 observations, J. Geophys. Res. Space Phys. 86 (A8) (1981) 6673–6684.

[14] B. Heber, T. Sanderson, M. Zhang, Corotating interaction regions, Adv. Space Res. 23 (3) (1999) 567–579.

[15] C. Russell, The Pioneer Venus Mission, in: Washington DC American Geophysical Union Geophysical Monograph Series, vol. 66, 1992, pp. 225–236.

[16] D. Titov, H. Svedhem, D. McCoy, J.-P. Lebreton, S. Barabash, J.-L. Bertaux, P. Drossart, V. Formisano, B. Haeusler, O. Korablev, et al., Venus express: Scientific goals, instrumentation, and scenario of the mission, Cosm. Res. 44 (4) (2006) 334–348.

[17] Y. Futaana, G. Stenberg Wieser, S. Barabash, J.G. Luhmann, Solar wind interaction and impact on the Venus atmosphere, Space Sci. Rev. 212 (3) (2017) 1453–1509.

[18] J. Luhmann, The solar wind interaction with Venus, Space Sci. Rev. 44 (3–4) (1986) 241–306.

[19] J. Luhmann, T. Cravens, Magnetic fields in the ionosphere of Venus, Space Sci. Rev. 55 (1–4) (1991) 201–274.

[20] L. Shan, Q. Lu, C. Mazelle, C. Huang, T. Zhang, M. Wu, X. Gao, S. Wang, The shape of the Venusian bow shock at solar minimum and maximum: Revisit based on VEX observations, Planet. Space Sci. 109 (2015) 32–37.

[21] Q. Xu, X. Xu, T. Zhang, Z. Rong, M. Wang, J. Wang, Y. Ye, Z. Zhou, Q. Chang, J. Xu, et al., The Venus express observation of Venus' induced magnetosphere boundary at solar maximum, Astron. Astrophys. 652 (2021) A113.

[22] M. Saunders, C. Russell, Average dimension and magnetic structure of the distant Venus magnetotail, J. Geophys. Res. Space Phys. 91 (A5) (1986) 5589–5604.

[23] T. Zhang, W. Baumjohann, M. Delva, H.-U. Auster, A. Balogh, C. Russell, S. Barabash, M. Balikhin, G. Berghofer, H. Biernat, H. Lammer, H. Lichtenegger, W. Magnes, R. Nakamura, T. Penz, K. Schwingenschuh, Z. Vörös, W. Zambelli, K.-H. Fornacon, K.-H. Glassmeier, I. Richter, C. Carr, K. Kudela, J. Shi, H. Zhao, U. Motschmann, J.-P. Lebreton, Magnetic field investigation of the Venus plasma environment: Expected new results from Venus express, Planet. Space Sci. 54 (13) (2006) 1336–1343, http://dx.doi.org/10.1016/j.pss.2006.04.018, The Planet Venus and the Venus Express Mission.

[24] S. Barabash, J.-A. Sauvaud, H. Gunell, H. Andersson, A. Grigoriev, K. Brinkfeldt, M. Holmström, R. Lundin, M. Yamauchi, K. Asamura, et al., The analyser of space plasmas and energetic atoms (ASPERA-4) for the Venus express mission, Planet. Space Sci. 55 (12) (2007) 1772–1792.

[25] C. Pollock, T. Moore, A. Jacques, J. Burch, U. Gliese, Y. Saito, T. Omoto, L. Avanov, A. Barrie, V. Coffey, J. Dorelli, D. Gershman, B. Giles, T. Rosnack, C. Salo, S. Yokota, M. Adrian, C. Aoustin, C. Auletti, S. Aung, V. Bigio, N. Cao, M. Chandler, D. Chornay, K. Christian, G. Clark, G. Collinson, T. Corris, A. De Los Santos, R. Devlin, T. Diaz, T. Dickerson, C. Dickson, A. Diekmann, F. Diggs, C. Duncan, A. Figueroa-Vinas, C. Firman, M. Freeman, N. Galassi, K. Garcia, G. Goodhart, D. Guererro, J. Hageman, J. Hanley, E. Hemminger, M. Holland, M. Hutchins, T. James, W. Jones, S. Kreisler, J. Kujawski, V. Lavu, J. Lobell, E. LeCompte, A. Lukemire, E. MacDonald, A. Mariano, T. Mukai, K. Narayanan, Q. Nguyan, M. Onizuka, W. Paterson, S. Persyn, B. Piepgrass, F. Cheney, A. Rager, T. Raghuram, A. Ramil, L. Reichenthal, H. Rodriguez, J. Rouzaud, A. Rucker, M. Samara, J.-A. Sauvaud, D. Schuster, M. Shappirio, K. Shelton, D. Sher, D. Smith, K. Smith, S. Smith, D. Steinfeld, R. Szymkiewicz, K. Tanimoto, J. Taylor, C. Tucker, K. Tull, A. Uhl, J. Vloet, P. Walpole, S. Weidner, D. White, G. Winkert, P.-S. Yeh, M. Zeuch, Fast plasma investigation for magnetospheric multiscale, Space Sci. Rev. 199 (1) (2016) 331–406, http://dx.doi.org/10.1007/s11214-016-0245-4.

[26] D. Vech, G. Stenberg, H. Nilsson, N.J.T. Edberg, A. Opitz, K. Szegő, T. Zhang, Y. Futaana, Statistical features of the global polarity reversal of the Venusian induced magnetosphere in response to the polarity change in interplanetary magnetic field, J. Geophys. Res. Space Phys. 121 (5) (2016) 3951–3962, http://dx.doi.org/10.1002/2015JA021995.

[27] J.A. Slavin, M.H. Acuña, B.J. Anderson, S. Barabash, M. Benna, S.A. Boardsen, M. Fraenz, G. Gloeckler, R.E. Gold, G.C. Ho, et al., MESSENGER and Venus Express observations of the solar wind interaction with Venus, Geophys. Res. Lett. 36 (9) (2009).

[28] T. Zhang, Q. Lu, W. Baumjohann, C. Russell, A. Fedorov, S. Barabash, A. Coates, A. Du, J. Cao, R. Nakamura, et al., Magnetic reconnection in the near Venusian magnetotail, Science 336 (6081) (2012) 567–570.

[29] E. Dubinin, M. Fraenz, J. Woch, T. Zhang, J. Wei, A. Fedorov, S. Barabash, R. Lundin, Bursty escape fluxes in plasma sheets of Mars and Venus, Geophys. Res. Lett. 39 (1) (2012).

[30] Z. Rong, S. Barabash, G. Stenberg, Y. Futaana, T. Zhang, W. Wan, Y. Wei, X. Wang, L. Chai, J. Zhong, The flapping motion of the Venusian magnetotail: Venus express observations, J. Geophys. Res. Space Phys. 120 (7) (2015) 5593–5602.

[31] P. Kollmann, P. Brandt, G. Collinson, Z. Rong, Y. Futaana, T. Zhang, Properties of planetward ion flows in Venus' magnetotail, Icarus 274 (2016) 73–82.

[32] V.K. Yadav, Plasma waves around Venus and Mars, IETE Tech. Rev. 38 (6) (2021) 622–661.

[33] F. Scarf, W. Taylor, I. Green, Plasma waves near Venus: Initial observations, Science 203 (4382) (1979) 748–750.

[34] L. Hadid, N.J. Edberg, T. Chust, D. Píša, A.P. Dimmock, A. Morooka, M. Maksimovic, Y.V. Khotyaintsev, J. Souček, M. Kretzschmar, et al., Solar Orbiter's first Venus flyby: Observations from the Radio and Plasma Wave instrument, Astron. Astrophys. 656 (2021) A18.

[35] C. Ho, R. Strangeway, C. Russell, Evidence for langmuir oscillations and a low density cavity in the Venus magnetotail, Geophys. Res. Lett. 20 (23) (1993) 2775–2778.

[36] M. Volwerk, T. Zhang, M. Delva, Z. Vörös, W. Baumjohann, K.-H. Glassmeier, First identification of mirror mode waves in Venus' magnetosheath? Geophys. Res. Lett. 35 (12) (2008).

[37] J. Eastwood, E. Lucek, C. Mazelle, K. Meziane, Y. Narita, J. Pickett, R. Treumann, The foreshock, Space Sci. Rev. 118 (2005) 41–94.

[38] T. Zhang, J. Du, Y. Ma, H. Lammer, W. Baumjohann, C. Wang, C. Russell, Disappearing induced magnetosphere at Venus: Implications for close-in exoplanets, Geophys. Res. Lett. 36 (20) (2009).

[39] M. Persson, S. Aizawa, N. André, S. Barabash, Y. Saito, Y. Harada, D. Heyner, S. Orsini, A. Fedorov, C. Mazelle, et al., BepiColombo mission confirms stagnation region of Venus and reveals its large extent, Nature Commun. 13 (1) (2022) 7743.

[40] Q. Xu, X. Xu, Q. Chang, Z. Rong, J. Wang, J. Xu, T. Zhang, Observations of the Venus dramatic response to an extremely strong Interplanetary Coronal Mass Ejection, Astrophys. J. 876 (1) (2019) 84.

[41] A.P. Dimmock, M. Alho, E. Kallio, S.A. Pope, T. Zhang, E. Kilpua, T.I. Pulkkinen, Y. Futaana, A.J. Coates, The response of the Venusian plasma environment to the passage of an ICME: Hybrid simulation results and Venus express observations, J. Geophys. Res. Space Phys. 123 (5) (2018) 3580–3601.

[42] D. Vech, K. Szego, A. Opitz, P. Kajdic, M. Fraenz, E. Kallio, M. Alho, Space weather effects on the bow shock, the magnetic barrier, and the ion composition boundary at Venus, J. Geophys. Res. Space Phys. 120 (6) (2015) 4613–4627.

[43] N.J. Edberg, H. Nilsson, Y. Futaana, G. Stenberg, M. Lester, S. Cowley, J. Luhmann, T. McEnulty, H.J. Opgenoorth, A. Fedorov, et al., Atmospheric erosion of Venus during stormy space weather, J. Geophys. Res. Space Phys. 116 (A9) (2011).

[44] N. Gopalswamy, A. Lara, S. Yashiro, S. Nunes, R.A. Howard, Coronal mass ejection activity during solar cycle 23, Solar Variab. Input Earth's Environ. 535 (2003) 403–414.

[45] P. Chen, Coronal mass ejections: models and their observational basis, Living Rev. Sol. Phys. 8 (2011) 1–92.

[46] J.B. Garvin, S.A. Getty, G.N. Arney, N.M. Johnson, E. Kohler, K.O. Schwer, M. Sekerak, A. Bartels, R.S. Saylor, V.E. Elliott, et al., Revealing the mysteries of Venus: The DAVINCI mission, Planet. Sci. J. 3 (5) (2022) 117.

[47] R.C. Ghail, C. Wilson, M. Galand, D. Hall, C. Cochrane, P. Mason, J. Helbert, F. MontMessin, S. Limaye, M. Patel, et al., EnVision: taking the pulse of our twin planet, Exp. Astron. 33 (2012) 337–363.

[48] S. Smrekar, S. Hensley, R. Nybakken, M.S. Wallace, D. Perkovic-Martin, T.-H. You, D. Nunes, J. Brophy, T. Ely, E. Burt, et al., VERITAS (Venus emissivity, radio science, InSAR, topography, and spectroscopy): a discovery mission, in: 2022 IEEE Aerospace Conference, AERO, IEEE, 2022, pp. 1–20.

[49] H. Auster, K. Glassmeier, W. Magnes, O. Aydogar, W. Baumjohann, D. Constantinescu, D. Fischer, K. Fornacon, E. Georgescu, P. Harvey, et al., The THEMIS fluxgate magnetometer, Space Sci. Rev. 141 (2008) 235–264.

[50] O. Le Contel, P. Leroy, A. Roux, C. Coillot, D. Alison, A. Bouabdellah, L. Mirioni, L. Meslier, A. Galic, M. Vassal, et al., The search-coil magnetometer for MMS, Space Sci. Rev. 199 (2016) 257–282.

[51] T. Karlsson, Y. Kasaba, J.-E. Wahlund, P. Henri, L. Bylander, W. Puccio, S.-E. Jansson, L. Åhlén, E. Kallio, H. Kojima, et al., The MEFISTO and WPT electric field sensors of the plasma wave investigation on the BepiColombo Mio spacecraft: measurements of low and high frequency electric fields at mercury, Space Sci. Rev. 216 (2020) 1–24.

[52] R. Ergun, S. Tucker, J. Westfall, K. Goodrich, D. Malaspina, D. Summers, J. Wallace, M. Karlsson, J. Mack, N. Brennan, et al., The axial double probe and fields signal processing for the MMS mission, Space Sci. Rev. 199 (2016) 167–188.

[53] J. McFadden, C. Carlson, D. Larson, M. Ludlam, R. Abiad, B. Elliott, P. Turin, M. Marckwordt, V. Angelopoulos, The THEMIS ESA plasma instrument and in-flight calibration, Space Sci. Rev. 141 (2008) 277–302.

[54] D. Delcourt, Y. Saito, F. Leblanc, C. Verdeil, S. Yokota, M. Fraenz, H. Fischer, B. Fiethe, B. Katra, D. Fontaine, et al., The mass spectrum analyzer (MSA) on board the BepiColombo MMO, J. Geophys. Res. Space Phys. 121 (7) (2016) 6749–6761.

[55] Y. Saito, D. Delcourt, M. Hirahara, S. Barabash, N. André, T. Takashima, K. Asamura, S. Yokota, M. Wieser, M.N. Nishino, et al., Pre-flight calibration and near-earth commissioning results of the mercury plasma particle experiment (MPPE) onboard MMO (Mio), Space Sci. Rev. 217 (2021) 1–91.

[56] K. Torkar, R. Nakamura, M. Tajmar, C. Scharlemann, H. Jeszenszky, G. Laky, G. Fremuth, K. Escoubet, K. Svenes, Active spacecraft potential control investigation, Space Sci. Rev. 199 (2016) 515–544.

[57] F. Mozer, DC and low-frequency double probe electric field measurements in space, J. Geophys. Res. Space Phys. 121 (11) (2016) 10–942.

[58] Y. Saito, J. Sauvaud, M. Hirahara, S. Barabash, D. Delcourt, T. Takashima, K. Asamura, M. BepiColombo, M. Team, et al., Scientific objectives and instrumentation of mercury plasma particle experiment (MPPE) onboard MMO, Planet. Space Sci. 58 (1–2) (2010) 182–200.

[59] S.Y. Karaoğlu, S. Karaoğlu, Ü. İmgesu, Aerospace industry and aluminum metal matrix composites, Int. J. Aviat. Sci. Technol. 2 (02) (2021) 73–81.

[60] T. Pradeep, S. Kumar Soni, B. Thomas, Design manufacture and testing of a composite support structure for spacecraft application, Mater. Today: Proc. 22 (2020) 1374–1379, http://dx.doi.org/10.1016/j.matpr.2020.01.459, URL https://www.sciencedirect.com/science/article/pii/S2214785320305642. 2nd International Conference on Materials Manufacturing and Modelling, ICMMM – 2019, VIT University, Vellore, 29th - 31st March 2019.

[61] S.M. Merkowitz, K.E. Castellucci, S.V. Depalo, J.A. Generie, P.G. Maghami, H.L. Peabody, Current LISA spacecraft design, J. Phys. Conf. Ser. 154 (1) (2009) 012021, http://dx.doi.org/10.1088/1742-6596/154/1/012021.

[62] L. Giulicchi, S.-F. Wu, T. Fenal, Attitude and orbit control systems for the LISA pathfinder mission, Aerosp. Sci. Technol. 24 (1) (2013) 283–294, http://dx.doi.org/10.1016/j.ast.2011.12.002, URL https://www.sciencedirect.com/science/article/pii/S127096381100201X, VFE-2.

[63] V.C. Thomas, J.M. Makowski, G.M. Brown, J.F. McCarthy, D. Bruno, J.C. Cardoso, W.M. Chiville, T.F. Meyer, K.E. Nelson, B.E. Pavri, D.A. Termohlen, M.D. Violet, J.B. Williams, The dawn spacecraft, Space Sci. Rev. 163 (1) (2011) 175–249, http://dx.doi.org/10.1007/s11214-011-9852-2.

[64] B.M. Jakosky, R.P. Lin, J.M. Grebowsky, J.G. Luhmann, D.F. Mitchell, G. Beutelschies, T. Priser, M. Acuna, L. Andersson, D. Baird, D. Baker, R. Bartlett, M. Benna, S. Bougher, D. Brain, D. Carson, S. Cauffman, P. Chamberlin, J.-Y. Chaufray, O. Cheatom, J. Clarke, J. Connerney, T. Cravens, D. Curtis, G. Delory, S. Demcak, A. DeWolfe, F. Eparvier, R. Ergun, A. Eriksson, J. Espley, X. Fang, D. Folta, J. Fox, C. Gomez-Rosa, S. Habenicht, J. Halekas, G. Holsclaw, M. Houghton, R. Howard, M. Jarosz, N. Jedrich, M. Johnson, W. Kasprzak, M. Kelley, T. King, M. Lankton, D. Larson, F. Leblanc, F. Lefevre, R. Lillis, P. Mahaffy, C. Mazelle, W. McClintock, J. McFadden, D.L. Mitchell, F. Montmessin, J. Morrissey, W. Peterson, W. Possel, J.-A. Sauvaud, N. Schneider, W. Sidney, S. Sparacino, A.I.F. Stewart, R. Tolson, D. Toublanc, C. Waters, T. Woods, R. Yelle, R. Zurek, The Mars atmosphere and volatile evolution (MAVEN) mission, Space Sci. Rev. 195 (1) (2015) 3–48, http://dx.doi.org/10.1007/s11214-015-0139-x.

[65] European Space Agency, Envision assessment study report, 2021, URL https://sci.esa.int/documents/34375/36249/EnVision_YB_final.pdf.